γ-soft shapes and quasiparticle excitations in $^{161}_{73}Ta_{88}$

K. Lagergren,[1,2,*] D. T. Joss,[1,3] E. S. Paul,[3] B. Cederwall,[2] J. Simpson,[1] D. E. Appelbe,[1] C. J. Barton,[1] S. Eeckhaudt,[4] T. Grahn,[4] P. T. Greenlees,[4] B. Hadinia,[2] P. Jones,[4] R. Julin,[4] S. Juutinen,[4] H. Kettunen,[4] M. Leino,[4] A.-P. Leppänen,[4] P. Nieminen,[4] R. D. Page,[3] J. Pakarinen,[4] J. Perkowski,[4,†] P. Rahkila,[4] C. Scholey,[4] J. Uusitalo,[4] D. D. Warner,[1] D. R. Wiseman,[3] and R. Wyss[2]

[1]*STFC Daresbury Laboratory, Daresbury, Warrington, WA4 4AD, United Kingdom*

[2]*Department of Physics, Royal Institute of Technology, S-10691 Stockholm, Sweden*

[3]*Oliver Lodge Laboratory, University of Liverpool, Liverpool, L69 7ZE, United Kingdom*

[4]*Department of Physics, University of Jyväskylä, P.O. Box 35, Jyväskylä FI-40014, Finland*

(Received 13 October 2010; published 26 January 2011)

Excited states in the neutron-deficient odd-Z nuclide ^{161}Ta were identified for the first time using the ^{106}Cd(^{58}Ni,3$p\gamma$) reaction at a beam energy of 270 MeV. The $\pi h_{11/2}$ band, yrast at low spin, was observed up to $(47/2^-)$ and a further four strongly coupled bands have been established to high spin. Quasiparticle configuration assignments for the new band structures have been made on the basis of cranked shell model calculations. This work suggests that the negative-parity $\nu(f_{7/2}, h_{9/2})$ orbitals are responsible for the first rotational alignment in the $\pi h_{11/2}$ band.

DOI: 10.1103/PhysRevC.83.014313 PACS number(s): 21.10.Re, 27.70.+q, 23.20.Lv

I. INTRODUCTION

The evolution of collective behavior in atomic nuclei has been of long-standing interest in nuclear physics. Quantal states in nuclei with proton and neutron numbers near closed shells are based on single-particle excitations. However, as valence nucleons are added to or removed from closed shells collective behavior arising from correlations between the constituent fermions emerges. Experimental evidence for such collective excitations includes the observation of regular γ-ray cascades originating from deformed nuclei rotating about a unique axis. The light Ta isotopes represent an ideal opportunity to investigate nuclear structure at the interface between the single-particle and collective regimes. The isotopic chain has been established from the spherical proton emitter ^{155}Ta, at the $N = 82$ shell closure [1,2], to the neutron-rich isotope ^{192}Ta [3]. The lightest Ta isotope for which a detailed level scheme has been established is ^{157}Ta [4]. In ^{157}Ta, multiplets of excited states are generated by coupling the spins of a small number of valence nucleons. With the addition of six neutrons, ^{163}Ta exhibits collective excitations manifested as strongly coupled bands observed up to $57/2\ \hbar$ [5]. Prior to this work, excited states had not been observed in the intermediate isotope ^{161}Ta, which lies between these single-particle and collective regimes.

For ^{161}Ta and the heavier isotopes, the proton Fermi level lies near the top of the $\pi h_{11/2}$ subshell and the yrast states are based on the odd proton occupying the high-Ω $[514]9/2^-$ state. The neutron Fermi surface occupies a region of low-Ω orbitals originating from the $f_{7/2}$, $h_{9/2}$, or $i_{13/2}$ subshells. This scenario where the proton and neutron Fermi surfaces lie at the top (high-Ω orbitals) or bottom (low-Ω orbitals) of their respective shells presents the ideal conditions for γ-soft or triaxial shapes. Such nuclei are sensitive to the occupation of core-polarizing orbitals at the Fermi surface. For example, the high-j, low-Ω $i_{13/2}$ neutrons have prolate core-polarizing tendencies and dominate the high-spin configurations of ^{163}Ta [5] and many other neutron-deficient nuclei in this mass region.

The Ta isotopes lying closer to the $N = 82$ shell closure are expected to be less deformed [6] and have the neutron $i_{13/2}$ orbital lying at higher excitation energies relative to their Fermi surface. Indeed, at $N = 88$, the neutron Fermi surface lies below the lowest Ω $i_{13/2}$ state, allowing the negative-parity $f_{7/2}/h_{9/2}$ states to have a greater influence on the yrast structure. This paper discusses the competing influences of the $\pi h_{11/2}$, $\nu f_{7/2}$, $\nu h_{9/2}$, and $\nu i_{13/2}$ orbitals on the observed structures in $^{161}Ta_{88}$.

II. EXPERIMENTAL DETAILS

The experiment was performed at the Accelerator Laboratory of the University of Jyväskylä, Finland. Excited states in ^{161}Ta were populated using the ^{106}Cd(^{58}Ni,3p) reaction at a beam energy of 270 MeV. The target consisted of a 0.9 mg/cm^2 thick, self-supporting ^{106}Cd foil of 96.5% isotopic enrichment. An average beam current of 6 pnA was used for an irradiation period of 6 days. Prompt γ rays were recorded at the target position by the JUROGAM γ-ray spectrometer [7] consisting of 43 EUROGAM escape-suppressed germanium spectrometers [8]. The recoiling fusion-evaporation residues were separated from the primary beam and fission products by the RITU gas-filled recoil separator [9] and implanted into the double-sided silicon strip detectors (DSSDs) of the GREAT spectrometer [10] at the focal plane. Recoiling evaporation residues were distinguished from the residual scattered beam and radioactive decays by energy loss and, in conjunction

*Present address: Joint Institute for Heavy Ion Research, Holifield Radioactive Ion Beam Facility, Oak Ridge, TN 37381, USA; karinl@ornl.gov.

†Also at Department of Nuclear Physics and Radiation Safety, University of Lodz, Pomorska, 149/153, PL-90-236, Lodz, Poland.

with the DSSDs, time-of-flight methods using the GREAT multiwire proportional counter. All detector signals were passed to the total data readout (TDR) acquisition system [11], where they were time stamped to a precision of 10 ns to allow accurate temporal correlations between γ rays detected at the target position, recoil implants, and their subsequent radioactive decays detected at the focal plane.

III. RESULTS

A. Assignment of γ rays to ^{161}Ta

The application of the recoil-decay tagging (RDT) technique [12–14], where prompt γ rays are correlated with the subsequent radioactive decays of specific nuclides, has been used to identify excited states in ^{157}Ta [4] and ^{159}Ta [15]. These nuclei have short α-decay half-lives and high branching ratios, which are ideal for the RDT technique. The α-decay properties of ^{161}Ta, however, are not optimal for identifying γ-ray transitions with RDT. The α-decay branch ($E_\alpha = 5147 \pm 10$ keV) [16–18] was estimated by Hofmann *et al.* to have a small branching ratio (∼5%) [18]. Moreover, the isotope has a relatively long half-life ($t_{1/2} = 2936 \pm 10$ ms) [16,17,19] compared with other reaction products. Recoil-decay correlations for ^{161}Ta were therefore problematic at the ion implantation rate used in the experiment owing to the increased probability of false correlations arising from multiple hits within the same DSSD pixel before the ^{161}Ta decay occurs. While it was not possible to perform an unambiguous identification of excited states in ^{161}Ta, it was still possible to bias these data even for these longer correlation times.

Recoil-decay correlations were analyzed using the GRAIN software package [20]. Figure 1(a) shows all γ rays correlated with implanted fusion residues in the GREAT spectrometer. The dashed lines indicate low-lying γ-ray transitions in ^{160}Hf [21] that are populated directly via the $4p$ fusion-evaporation channel. Figure 1(b) shows the γ rays observed by demanding correlations with ion implantations followed by the $\alpha(^{161}\text{Ta})$-$\alpha(^{157}\text{Lu})$ decay chain within the same DSSD pixel. The γ rays from transitions in ^{160}Hf are still visible in the decay-tagged spectrum but the relative intensities are lower compared with the nearby 396-, 483-, 600-, and 680-keV transitions, which are assigned as transitions in ^{161}Ta. The 483-keV transition is the most prominent γ ray in Fig. 1(a), which is consistent with the expectation that the $3p$ evaporation channel to ^{161}Ta should be the most intensely populated at the bombarding energy employed. Indeed, the PACE4 fusion evaporation code [22,23] predicts relative yields for ^{162}W($2p$), ^{161}Ta($3p$), and ^{160}Hf($4p$) reaction products as 3%, 12%, and 3% of the total reaction cross section, respectively.

B. γ-ray coincidence analysis

A total of 4.1×10^7 threefold and higher coincidences were recorded in delayed coincidence with any recoil implanted in the DSSDs. These data were sorted off-line using GRAIN [20] and other software packages into an $E_{\gamma 1}$-$E_{\gamma 2}$-$E_{\gamma 3}$ coincidence cube, which was analyzed using the LEVIT8R graphical analysis software package [24]. The level scheme for ^{161}Ta was constructed using relative γ-ray intensities and coincidence relationships from spectra generated from this cube. The deduced level scheme for ^{161}Ta is displayed in Fig. 2 and the properties of γ rays assigned to this nucleus are recorded in Table I. Typical double-gated coincidence spectra are displayed in Fig. 3.

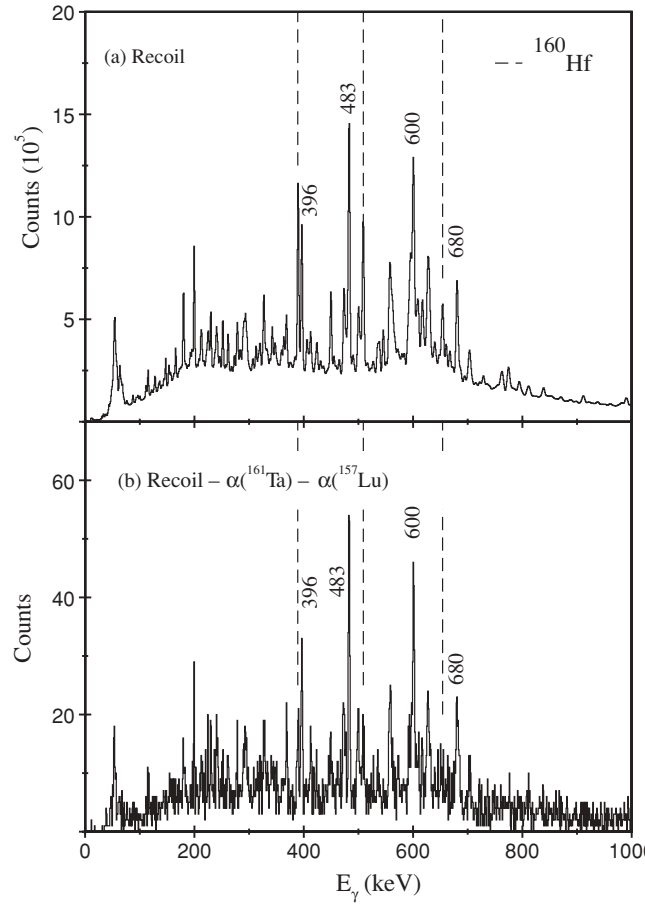

FIG. 1. (a) γ-ray transitions correlated with any fusion-evaporation residue implanted in the GREAT spectrometer. (b) γ rays correlated with an implanted ion and followed by an α decay of ^{161}Ta decay within 3 s and a subsequent α decay of ^{157}Lu within 3 s of the first α decay in the same DSSD pixel. The dotted line indicates the location of the 399-, 509-, and 654-keV γ rays in ^{160}Hf [21]. Transitions assigned to ^{161}Ta are labeled by their energies in keV.

Multipolarity assignments for the γ-ray transitions were obtained from measurements of angular-intensity ratios using the method of directional correlations from oriented states (DCOs) [25]. Multipolarities were extracted from intensity ratios of coincident γ rays observed in detectors at backward ($\theta = 158°$) and perpendicular ($\theta = 86°$ or $94°$) angles, relative to the beam direction, according to the relation

$$R_{\text{DCO}} = \frac{I_{\text{backward}}[\text{gated perpendicular}]}{I_{\text{perpendicular}}[\text{gated backward}]}. \quad (1)$$

C. Level scheme of ^{161}Ta

The strongest band, band 1, is assigned to be based on the proton $h_{11/2}$ state and is established to $I^\pi = (47/2^-)$ and an excitation energy of $E_x = 6092$ keV relative to the

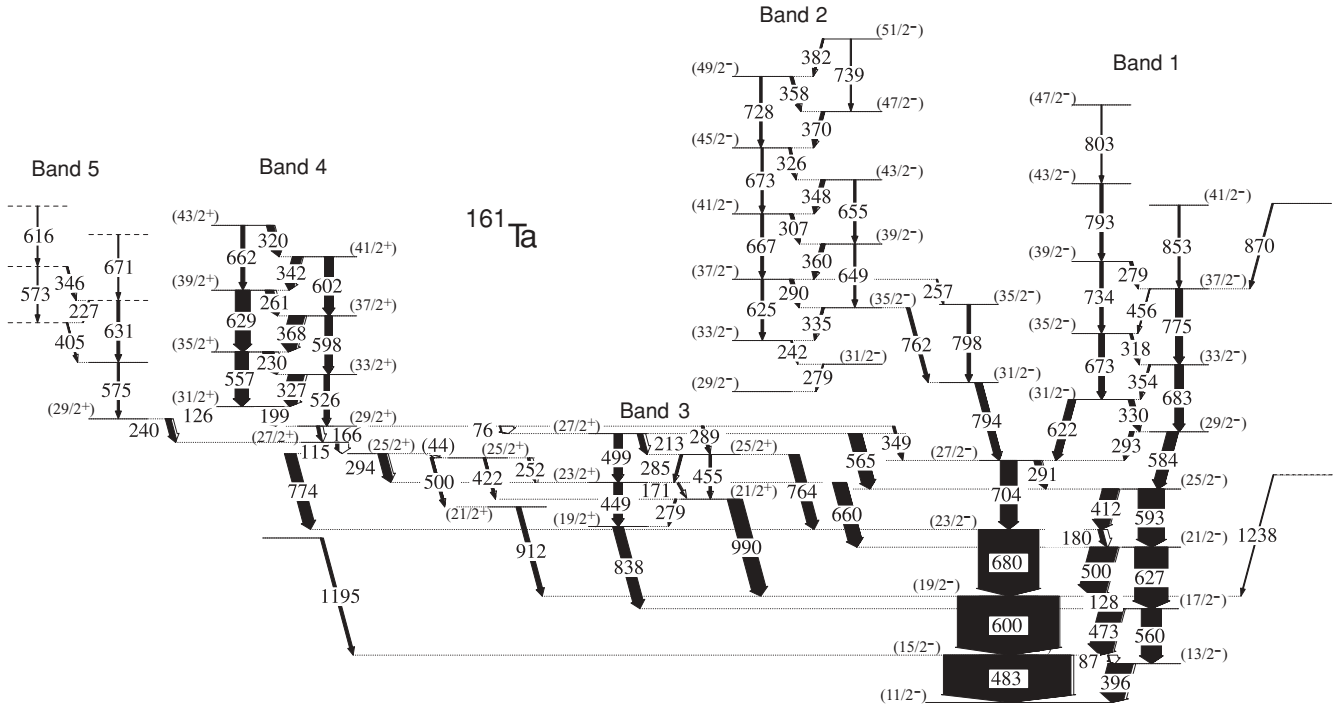

FIG. 2. Level scheme deduced for ^{161}Ta. The transition energies are given in keV and their measured relative intensities are proportional to the widths of the arrows. Dashed lines and parentheses indicate tentative assignments.

$11/2^-$ state. Figure 3(a) shows γ rays in coincidence with the 584- and 593-keV transitions highlighting γ-ray transitions assigned to band 1. The $R_{\rm DCO}$ values in this strongly coupled band distinguish between the in-band stretched quadrupole and interband $\Delta I = 1$ ($M1/E2$) interleaving γ rays, respectively. At low spin, band 1 is expected to have the same structure as the yrast bands established in the heavier odd-A Ta isotopes, which are based on the odd proton occupying the $[514]9/2^-$ Nilsson orbital. In ^{161}Ta, the γ-ray transitions to the $9/2^-$ bandhead are not observed. Transitions between the low-spin states of the $\alpha = +1/2$ signature of band 1 have lower intensities relative to the interleaving $\Delta I = 1$ transitions and the in-band $13/2^- \rightarrow 9/2^-$ transition is likely to be much weaker than the 396-keV dipole transition. Furthermore, trends in the light Ta isotopes indicate that the energy difference between the $11/2^-$ state and the $9/2^-$ bandhead becomes very small toward $N = 88$. Indeed, the measured energy differences for ^{167}Ta [26], ^{165}Ta [27], and ^{163}Ta [5] are 99, 71, and 45 keV, respectively. Assuming the trend extrapolates to ^{161}Ta, the decay to the $9/2^-$ state via a low-energy $M1$ transition is more likely to proceed by internal conversion than by γ-ray emission.

Band 1 is fed by another weakly populated, strongly coupled band (band 2) via the 257-, 762-, 798-, and 794-keV transitions. Figure 3(b) shows a coincidence spectrum generated by demanding coincidences with 290- and 360-keV γ rays showing transitions in band 2.

The strongest excited band structures are labeled bands 3 and 4 in Fig. 2. Figure 3(c) shows γ rays assigned to band 4 generated by demanding coincidences with the 166- and 199-keV transitions. Figure 3(c) indicates that band 4 feeds the low-spin states of band 1 via a further strongly coupled band (band 3). The tentative 44-keV transition that connects two (25/2) states was not observed but was inferred from coincidence relations between other γ rays. The 115- and 294-keV transitions linking bands 3 and 4 are measured to have $R_{\rm DCO}$ values of 0.88(10) and 0.69(13), respectively, which are consistent with dipole transitions.

Particle-rotor calculations based on the semiclassical model of Dönau and Frauendorf [28,29] predict that configurations with an odd proton in an $h_{11/2}$ orbital should have positive multipole mixing ratios, $\delta_{E2/M1}$, for the $\Delta I = 1$ transitions. This could be manifested experimentally as larger $R_{\rm DCO}$ values ($\sim$0.8) for interleaving transitions within the strongly coupled bands. Thus, the connecting dipole transitions are assigned $M1/E2$ multipolarities, while the transitions linking band 3 to band 1 are assigned as $E1$ transitions on the basis of the lower $R_{\rm DCO}$ ratios ($R_{\rm DCO} \sim 0.5$). This constrains band 3 and band 4 to be based on positive-parity configurations.

Figure 3(d) shows evidence for a weakly populated strongly coupled structure, band 5. It has not been possible to determine DCO ratios for transitions within band 5 and therefore only a tentative initial spin-parity of $(29/2^+)$ is indicated in Fig. 2 (see the discussion below).

IV. DISCUSSION

To elucidate the underlying configuration assignments of the band structures, these experimental data are presented in terms of the aligned angular momentum, i_x, as a function of rotational frequency. The aligned angular momentum (or

TABLE I. Measured properties of γ-ray transitions assigned to ^{161}Ta. Energies are accurate to ± 0.5 keV for the strong transitions ($I_\gamma \gg 10\%$) rising to ± 2.0 keV for the weaker transitions.

E_γ (keV)	I_γ (%)	R_{DCO}	Band	Multipolarity
75.8	1.0(1)		$4 \rightarrow 3$	
86.9	1.0(1)	0.5(4)	1	$M1/E2$
114.9	2.6(1)	0.9(1)	$4 \rightarrow 3$	$M1/E2$
125.6	0.2(1)		$4 \rightarrow 5$	
127.5	1.7(10)	0.6(2)	1	$M1/E2$
165.6	2.4(1)	0.9(1)	$4 \rightarrow 3$	$E2$
170.7	0.9(1)	0.5(3)	3	$M1/E2$
180.0	3.7(17)	0.8(2)	1	$M1/E2$
199.3	12.3(5)	0.9(1)	4	$M1/E2$
213.4	4.2(2)	0.6(1)	3	$M1/E2$
227.1	0.6(1)		5	
229.9	8.6(4)	0.9(1)	4	$M1/E2$
240.0	4.4(3)		$5 \rightarrow 4$	
241.8	0.9(1)		2	
251.7	2.3(2)	1.0(1)	$4 \rightarrow 3$	$M1/E2$
256.7	0.6(1)		$2 \rightarrow 1$	
261.4	6.5(3)	0.7(1)	4	$M1/E2$
278.6	2.0(1)		1	
278.7	0.8(1)		2	
278.7	1.4(2)	1.1(1)	3	$M1/E2$
285.4	1.7(1)	0.7(2)	3	$M1/E2$
288.8	1.9(1)	1.2(4)	$4 \rightarrow 3$	$E2$
289.6	1.9(1)	0.6(2)	2	$M1/E2$
291.1	3.2(2)		1	
293.0	2.9(2)	0.8(2)	1	$M1/E2$
293.7	6.5(3)	0.7(1)	$4 \rightarrow 3$	$M1/E2$
307.2	2.4(2)	0.5(2)	2	$M1/E2$
318.4	1.7(1)		1	
320.1	5.5(2)	0.8(1)	4	$M1/E2$
325.5	1.6(2)	0.8(2)	2	$M1/E2$
327.1	12.2(6)	0.8(1)	4	$M1/E2$
329.6	3.7(3)	0.7(1)	1	$M1/E2$
334.5	1.7(1)		2	
341.9	7.3(4)	0.7(1)	4	$M1/E2$
346.4	1.2(1)		5	
347.7	2.9(2)	0.4(1)	2	$M1/E2$
349.2	2.0(1)	0.7(3)	$4 \rightarrow 1$	$E1$
354.2	1.2(1)		1	
358.2	2.2(2)		2	
359.8	3.0(2)	0.5(1)	2	$M1/E2$
368.0	12.0(5)	0.7(1)	4	$M1/E2$
370.3	2.5(2)		2	
382.1	1.2(1)		2	
396.1	19.2(9)	0.9(1)	1	$M1/E2$
405.3	1.0(1)		5	
412.4	12.3(6)	0.7(1)	1	$M1/E2$
422.0	1.7(2)		$4 \rightarrow 3$	
449.2	6.5(4)	1.0(1)	3	$E2$
454.7	1.9(2)	1.3(4)	3	$E2$
455.8	0.7(2)		1	
473.3	18.6(10)	1.0(2)	1	$M1/E2$
482.7	100.0(3)	0.9(1)	1	$E2$
498.7	6.3(3)	0.9(1)	3	$E2$
499.7	1.3(3)		$4 \rightarrow 3$	
500.4	21.1(1)	0.9(1)	1	$M1/E2$
526.3	4.1(3)		4	
557.0	10.2(5)		4	
560.4	15.5(8)	1.1(1)	1	$E2$
565.4	10.2(5)	0.6(1)	$3 \rightarrow 1$	$E1$
572.8	0.9(2)		5	
575.3	1.7(2)		5	
583.6	8.9(5)	1.2(1)	1	$E2$
593.0	20.4(10)	1.0(1)	1	$E2$
598.0	5.5(4)		4	
600.4	79.4(36)	1.1(1)	1	$E2$
602.3	6.6(4)		4	
616.0	0.8(2)		5	
622.0	8.5(6)		1	
624.6	1.6(2)		2	
627.1	25.9(12)		1	
629.0	11.4(6)		4	
631.2	2.2(2)		5	
649.4	1.6(2)		2	
654.7	0.6(2)		5	
660.4	10.7(6)		$3 \rightarrow 1$	
661.6	3.2(3)		4	
666.7	2.2(2)		2	
671.5	0.8(2)		5	
672.5	4.3(3)		1	
673.2	1.8(2)		2	
680.2	47.1(20)	1.1(1)	1	$E2$
683.0	6.6(4)	1.0(1)	1	$E2$
704.1	12.9(7)	1.1(1)	1	$E2$
728.0	1.9(4)		2	
734.4	2.6(2)		1	
739.0	1.0(2)		2	
761.9	2.7(2)	1.1(4)	$2 \rightarrow 1$	$E2$
764.4	8.1(6)	0.7(1)	$3 \rightarrow 1$	$E1$
773.9	8.8(5)		$4 \rightarrow 1$	
774.6	5.5(3)	1.1(3)	1	$E2$
793.5	8.0(12)		1	
798.0	2.8(3)		$2 \rightarrow 1$	
803.2	0.9(2)		1	
838.3	8.2(6)	0.4(1)	$3 \rightarrow 1$	$E1$
852.8	1.6(2)		1	
870.4	1.3(1)		$\rightarrow 1$	
911.5	3.7(6)	0.4(2)	$4 \rightarrow 1$	$E1$
990.0	11.5(5)	0.6(1)	$3 \rightarrow 1$	$E1$
1194.6	2.5(2)		$\rightarrow 1$	
1238.0	0.8(1)		$\rightarrow 1$	

alignment) [30] is defined as

$$i_x = \sqrt{I(I+1) - K^2} - I_{\mathrm{Ref}}, \tag{2}$$

where I is the spin of the excited state, K is the angular momentum projection along the nuclear symmetry axis, and

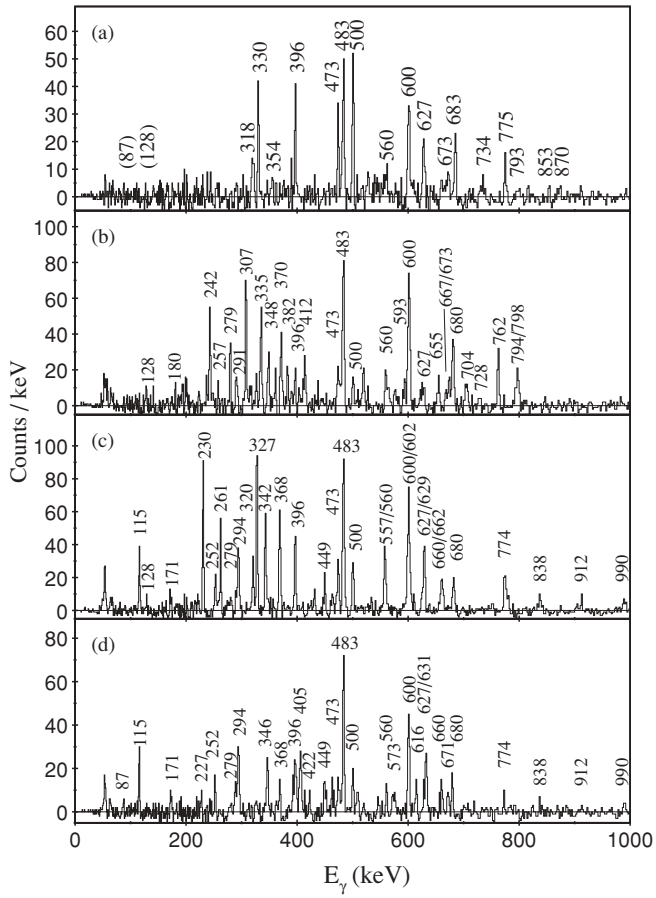

FIG. 3. Typical γ-ray coincidence spectra extracted from a recoil-gated γ^3 cube. (a) γ rays in coincidence with 584- and 593-keV transitions showing transitions in band 1. (b) γ rays in coincidence with 290- and 360-keV transitions showing transitions in band 2. (c) γ rays in coincidence with 166- and 199-keV γ rays showing transitions in band 4 and its decay path to band 1 via band 3. (d) γ rays in coincidence with 240- and 575-keV transitions showing transitions in band 5 and the decay path to band 1.

$I_{\rm Ref}$ is a rotational reference defined by the Harris parameters [31] such that

$$I_{\rm Ref} = \mathcal{J}_0\omega + \mathcal{J}_1\omega^3. \quad (3)$$

A rotational reference, based on a configuration with a variable moment of inertia defined by the Harris parameters $\mathcal{J}_0 = 26\,\hbar^2$ MeV^{-1} and $\mathcal{J}_1 = 32\,\hbar^4$ MeV^{-3}, has been subtracted from each band. The Harris parameters were chosen to give an almost constant alignment for band 1 at low spin. Figures 4(a) and 4(b) show the experimental alignments for bands in ^{161}Ta and ^{163}Ta, respectively.

Figure 4(a) shows that band 1 in ^{161}Ta undergoes a gain in alignment gain of $\Delta i_x \sim 6\,\hbar$ at $\hbar\omega = 0.3$ MeV. The alignment gain is markedly different to the rotational alignment observed at a similar rotational frequency for band 1 in ^{163}Ta [see Fig. 4(b)]. This alignment gain of $\Delta i_x \sim 11\hbar$ is attributed to the rotational alignment of an $i_{13/2}$ neutron pair [5] and is also established in the analogous $h_{11/2}$ bands in the heavier odd-A isotopes [26,27,32].

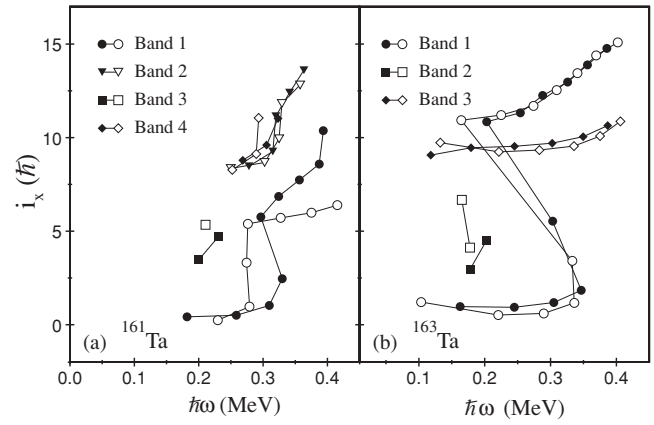

FIG. 4. Experimental alignments extracted for strongly coupled bands in (a) ^{161}Ta and (b) ^{163}Ta [5]. Solid (open) symbols refer to the $\alpha = -1/2$ ($\alpha = +1/2$) signature. A rotational reference, based on a configuration with a variable moment of inertia defined by the Harris parameters $\mathcal{J}_0 = 26\,\hbar^2$ MeV^{-1} and $\mathcal{J}_1 = 32\,\hbar^4$ MeV^{-3}, has been subtracted from each band.

Similar differences in alignment are noted between the isotones ^{162}W [33] and ^{164}W [34]. In ^{162}W the lowest two-quasiparticle excitation has a lower degree of alignment ($\Delta i_x \sim 6\hbar$) than that observed for the aligned $(\nu i_{13/2})^2$ configuration of ^{164}W ($\Delta i_x \sim 11\hbar$). Dracoulis *et al.* interpreted the lower alignment as evidence for $h_{9/2}$ neutron alignment [33]. Indeed, studies of the intervening odd-N isotope, ^{163}W, have revealed that the $h_{9/2}$ neutron pair alignment is favored as the first rotational alignment over the unblocked $i_{13/2}$ crossing [35]. This can be explained in terms of the transition to lower average deformations as the $N = 82$ closed shell is approached [33,35]. At lower deformations the low-Ω $\nu i_{13/2}$ orbital lies at higher excitation energy relative to the low-lying negative-parity states and the Fermi surface, thereby allowing the $h_{9/2}$ neutron orbitals to form the first rotational alignment. The same scenario is envisaged for ^{161}Ta and the lower alignment gain in band 1 is attributed to the $h_{9/2}$, $f_{7/2}$ neutron orbitals.

The alignments of band 1 in ^{161}Ta exhibit a difference in the crossing frequency for each signature and have different gradients above the first band crossing. This is in contrast to ^{163}Ta where the crossing frequency and alignment properties above the crossing are almost identical.

The unusual features of ^{161}Ta may originate from changes in the triaxial deformation. Triaxial or γ-soft nuclear shapes can promote large signature splitting in deformation aligned (high-Ω) orbitals at low rotational frequencies [36]. Such splitting can lead to different alignments for each signature of the $h_{11/2}$ state upon which band 1 is built. Figure 5 compares the signature splitting of the $h_{11/2}$ bands in ^{161}Ta and the heavier isotopes (^{163}Ta [5] and ^{165}Ta [27]) in terms of the staggering parameter $S(I)$ [37] defined as

$$S(I) = E(I) - E(I-1) - 1/2[E(I+1) - E(I) + E(I-1) - E(I-2)]. \quad (4)$$

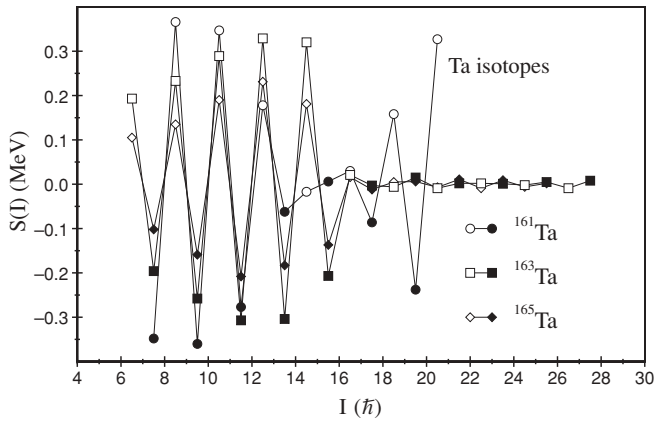

FIG. 5. Staggering parameter $S(I)$ as a function of spin I for the $[514]9/2^-$ bands in the neutron-deficient odd-A tantalum isotopes ^{161}Ta, ^{163}Ta, and ^{165}Ta. The solid (open) symbols represent the $\alpha = -1/2\ (+1/2)$ signatures.

At low spin each isotope exhibits large signature splitting. Similar behavior has been observed in the odd-Z Ir [38,39] and Re [40,41] isotopes and has been interpreted as resulting from a triaxial deformation generated by the competing core polarizing influences of the high-Ω $h_{11/2}$ proton and the low-Ω neutron orbitals. At high spin, the staggering parameter becomes very small in the $N \geqslant 90$ tantalum isotopes reflecting the dramatic reduction in signature splitting. The observed reduction has been interpreted in terms of a shape transition from γ-soft triaxial to axially symmetric prolate deformations brought about by the rotational alignment of a pair of $i_{13/2}$ neutrons [5,39–41]. In marked contrast to the heavier Ta isotopes, the signature splitting in band 1 of ^{161}Ta persists beyond the first rotational alignment. This is consistent with the weaker core polarization of the aligned $(\nu h_{9/2}, f_{7/2})^2$ orbitals.

Further insights into the changing structure of the $\pi h_{11/2}$ bands in the light Ta isotopes can be made by considering the total energy of the nuclei in the rotating frame (or total Routhian, E'). The total Routhians have been calculated for multi-quasiparticle configurations by summing single-particle Routhians extracted from cranked-shell model calculations incorporating a Nilsson potential and adding a γ-deformation-dependent reference as proposed by Frauendorf and May [42,43] such that

$$E'(\omega,\gamma) = \sum_{\mu} e'_{\mu}(\omega,\gamma) + E'_{\mathrm{Ref}}(\omega,\gamma), \tag{5}$$

where e'_{μ} are the single-particle energies. The γ-dependent reference is determined using the function

$$E'_{\mathrm{Ref}}(\omega,\gamma) = \tfrac{1}{2}V_{\mathrm{po}}\cos(3\gamma) - \tfrac{2}{3}\omega^2\left(\mathcal{J}_0 + \tfrac{1}{2}\omega^2\mathcal{J}_1\right)\cos^2(\gamma + 30^\circ), \tag{6}$$

where V_{po} is a prolate-oblate energy difference and $\mathcal{J}_0$ and $\mathcal{J}_1$ are the Harris parameters used to calculate the alignments. The total Routhians for ^{163}Ta and ^{161}Ta are shown in Figs. 6(a) and 6(b). The Routhians are calculated at a rotational frequency of 0.2 MeV and assume a prolate-oblate energy difference

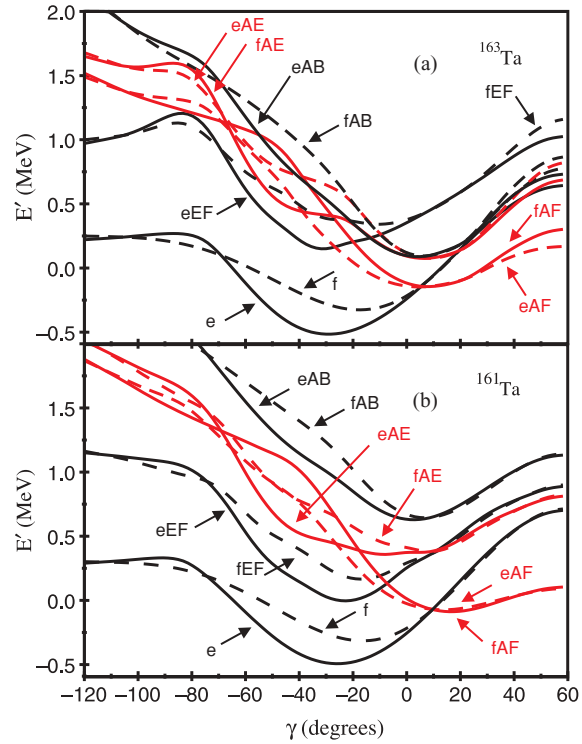

FIG. 6. (Color online) Calculated total Routhians as a function of γ deformation for single- and three-quasiparticle configurations in the light Ta isotopes at a rotational frequency of 0.2 MeV. (a) Calculations for ^{163}Ta assuming deformation parameters $\varepsilon_2 = 0.158$ and $\varepsilon_4 = 0.007$. (b) Calculations for ^{161}Ta assuming deformation parameters $\varepsilon_2 = 0.133$ and $\varepsilon_4 = -0.007$. The deformation parameters are taken from Ref. [6]. The e, f, eAB, fAB, eEF, and fEF configurations have overall negative parity (black lines) while the eAE, fAE, eAF, and fAF configurations have overall positive parity (red lines). The solid (dashed) lines represent the $\alpha = -1/2(+1/2)$ signatures.

$V_{\mathrm{po}} = -0.4$ MeV. The labeling convention for the constituent quasiparticles, adopted from Ref. [44], is listed in Table II.

The microscopic basis for the observed features of band 1 in ^{161}Ta and ^{163}Ta can be gleaned from Fig. 6. The single-quasiparticle configurations, labeled e and f, represent the

TABLE II. Convention for the quasiparticle labeling, taken from [44].

Label	(Parity, Signature) (π,α)	Main shell model component
	Quasineutrons	
A	$(+,+1/2)_1$	$i_{13/2}$
B	$(+,-1/2)_1$	$i_{13/2}$
C	$(+,+1/2)_2$	$i_{13/2}$
E	$(-,-1/2)_1$	$h_{9/2}, f_{7/2}$
F	$(-,+1/2)_1$	$h_{9/2}, f_{7/2}$
	Quasiprotons	
e	$(-,-1/2)_1$	$h_{11/2}$
f	$(-,+1/2)_1$	$h_{11/2}$

two signatures of the negative-parity $h_{11/2}$ proton orbital in both nuclei. There is a large degree of signature splitting between the e and f Routhians in the range $-70^\circ \leqslant \gamma \leqslant -10^\circ$, which is consistent with the experimental staggering parameter extracted for both isotopes at low spin, as shown in Fig. 5. The alignment gain observed in the $h_{11/2}$ band in both nuclei is indicative of the transition to a three-quasiparticle structure. Moreover, the measured $R_{\rm DCO}$ ratios constrain the high-spin states of band 1 in each isotope to have negative parity, thereby restricting the structure to be either the $\pi h_{11/2} \otimes (h_{9/2}, f_{7/2})^2$ (eEF/fEF) or $\pi h_{11/2} \otimes (i_{13/2})^2$ (eAB/fAB) configuration. Figure 6(a) indicates that, in ^{163}Ta, the eAB/fAB configurations are the lowest-energy negative-parity structures at $\gamma = 15^\circ$ and are predicted to have zero signature splitting, which is consistent with the staggering parameter at high spin ($I > 15\hbar$) displayed in Fig. 5. In contrast, Fig. 6(b) shows that the lowest-energy negative-parity three-quasiparticle structures in ^{161}Ta are the eEF/fEF configurations. In addition, the eEF and fEF total Routhians exhibit large signature splitting and have energy minima at different γ deformations, $\gamma = -25^\circ$ and $\gamma = -10^\circ$, respectively. This assignment is congruous with the low alignment gain observed for ^{161}Ta ($\Delta i_x = 6\hbar$) relative to ^{163}Ta ($\Delta i_x = 11\hbar$). The total Routhian calculations shown in Fig. 6(b) predict significant signature splitting between the eEF and fEF structures, as is observed in the staggering parameter extracted for ^{161}Ta at high spin.

Figure 4(a) shows that band 2 also carries an alignment consistent with a three-quasiparticle structure. Band 2 is assigned to be a negative-parity structure on the basis of angular intensity measurements. Figure 6(b) indicates that the next available negative-parity configuration is the eAB/fAB configuration based on aligning a pair of $i_{13/2}$ neutrons. The relatively high excitation energy of band 2 is consistent with the predicted total Routhians for the eAB/fAB structures and reflects the distance of the $\nu i_{13/2}$ orbital from the Fermi surface. Band 2 shows an increase in alignment at $\hbar\omega = 0.3$ MeV, which indicates the transition from a three-quasiparticle to a five-quasiparticle band structure. The five-quasiparticle configurations are likely to be the eABEF/fABEF formed by coupling the odd $h_{11/2}$ proton to rotationally aligned $i_{13/2}$ and $h_{9/2}$, $f_{7/2}$ neutron pairs.

Figure 6 indicates that the remaining excited bands in ^{163}Ta and ^{161}Ta are likely to be positive-parity three-quasiparticle configurations. Figure 4(a) shows that band 3 carries an alignment of only $\sim 5\hbar$ at 0.25 MeV/$\hbar$, which is too low for a positive-parity three-quasiparticle structure. Band 3 has similar alignment characteristics to the $\pi h_{11/2} \otimes 3^-$ octupole excitation in ^{163}Ta and is likely to have the same underlying configuration. The strongly populated positive-parity structure, band 4, is assigned to be the eAF/fAF configuration on the basis of the calculated Routhians and its alignment characteristics. Indeed, total Routhian calculations performed at the higher rotational frequency of $\hbar\omega = 0.3$ MeV indicate that the eAF/fAF configurations are clearly the lowest-energy three-quasiparticle structures. A similar band has also been established in ^{163}Ta.

The strongly coupled band, band 5, is weakly populated and DCO ratios could not be deduced. Figure 6(b) predicts that the positive-parity eAE/fAE configuration lies at similar excitation

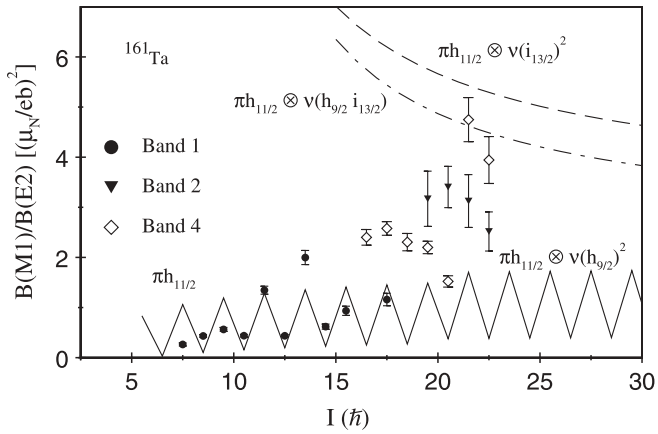

FIG. 7. Experimental $B(M1: I \to I-1)/B(E2: I \to I-2)$ ratios of reduced transition strength ratios as a function of spin I for ^{161}Ta. Measured values are compared with the predictions of the semiclassical model of Dönau and Frauendorf for the $\pi h_{11/2}$ configuration and the aligned $\pi h_{11/2} \otimes \nu(h_{9/2})^2$ (solid line), $\pi h_{11/2} \otimes \nu(h_{9/2}, i_{13/2})$ (dot-dashed line), and $\pi h_{11/2} \otimes \nu(i_{13/2})^2$ (dashed line) configurations. Band 1 is represented by solid circles, band 2 by solid triangles, and band 4 by open diamonds.

energies to the other three-quasiparticle configurations. Thus, the eAE/fAE configuration is a candidate for the underlying configuration of band 5. Based on the assumed bandhead spin of (29/2) its alignment is also consistent with this assignment.

To provide additional confirmation of the configuration assignments the $B(M1: I \to I-1)/B(E2: I \to I-2)$ ratios of reduced transition probabilities have been measured. These ratios have been extracted from experimental γ-ray branching ratios of competing $\Delta I = 1$ and $\Delta I = 2$ transitions and compared with the predictions of the semiclassical formalism of Dönau and Frauendorf [28,29] (see Fig. 7). The calculations assume a quadrupole deformation of $\beta_2 = 0.143$ [6]. Experimental alignments were extracted from Fig. 4, while g factors were obtained from cranked Woods-Saxon calculations.

The calculations for the configurations of band 1 (solid line) assume a γ deformation of -30° and a nonzero signature splitting term. The experimental ratios for band 1 are in reasonable agreement with theoretical predictions for the odd proton $h_{11/2}$ in a deformation aligned orbital. Thus, band 1 in ^{161}Ta is confirmed as a $h_{11/2}$ configuration formed by placing the odd proton in the [514]9/2$^-$ Nilsson state as observed in the heavier isotopes [5,27]. It should be noted that the calculations for band 1 assume a significant γ deformation of $\gamma = -30^\circ$ to provide a reasonable fit to these data, implying that band 1 is based on an odd proton coupled to a triaxial core as predicted by the total Routhian calculations. The measured $B(M1: I \to I-1)/B(E2: I \to I-2)$ ratios for the excited band configurations, bands 2 and 4, are larger than those measured for band 1. Figure 7 compares these experimental ratios with calculations for the three-quasiparticle $\pi h_{11/2} \otimes \nu(i_{13/2})^2$ and $\pi h_{11/2} \otimes \nu(h_{9/2}, i_{13/2})$ configurations. The poor agreement with the experimental values might arise from the assumptions that the excited bands are based on configurations that have the same β_2 deformation, axial symmetry and pure single-particle configurations. However, the calculations predict the correct

relative ordering of configurations with bands 2 and 4 assigned as the odd $h_{11/2}$ proton coupled to the aligned $\nu(i_{13/2})^2$ and $\nu(h_{9/2}, i_{13/2})$ configurations, respectively.

V. CONCLUSION

Five new strongly coupled band structures have been observed in the neutron-deficient nucleus ^{161}Ta using the JUROGAM and GREAT spectrometers in conjunction with the RITU gas-filled separator. Configuration assignments for all the new bands have been proposed based on the variation of the aligned angular momenta as a function of rotational frequency and ratios of reduced transition probabilities. The first alignment in the yrast $h_{11/2}$ band is attributed to the rotational alignment of the negative-parity EF $(h_{9/2}, f_{7/2})$ quasineutrons. This is preferred over the AB $(i_{13/2})^2$ alignment observed in the heavier isotopes owing to the lower average deformation of ^{161}Ta. Comparisons of experimental signature splitting, as highlighted by the staggering parameter, with the predictions of total Routhian calculations suggest that γ-soft triaxial shapes persist after the rotational alignment of the $(h_{9/2}, f_{7/2})$ quasineutrons. This constitutes a marked difference from the heavier Ta isotopes, which show zero splitting after the rotational alignment and is suggested to arise from the weaker core polarization of the $\nu(h_{9/2}, f_{7/2})$ orbitals relative to the $\nu i_{13/2}$ orbitals.

ACKNOWLEDGMENTS

The authors would like to express their gratitude to the staff of the Accelerator Laboratory at the University of Jyväskylä for their excellent technical support. The authors also thank Paul Morrall of Daresbury Laboratory for the preparation of the Cd targets. Financial support for this work has been provided by the UK Science and Technology Facilities Council (STFC), the EU 6th Framework Programme, Integrating Infrastructure Initiative-Transnational Access (EURONS, Contract No. 506065), the Academy of Finland under the Finnish Centre of Excellence Programme 2006–2011, and by the Swedish Research Council. K.L. would like to acknowledge the support of the Royal Society. P.T.G., C.S., and P.N. acknowledge the support of the Academy of Finland (Contracts No. 111965, No. 209430, and No. 121110). We thank the UK/France (STFC/IN2P3) Loan Pool and the GAMMAPOOL European Spectroscopy Resource for the loan of detectors for JUROGAM.

[1] J. Uusitalo *et al.*, Phys. Rev. C **59**, R2975 (1999).
[2] R. D. Page *et al.*, Phys. Rev. C **75**, 061302R (2007).
[3] N. Alkhomashi *et al.*, Phys. Rev. C **80**, 064308 (2009).
[4] D. Seweryniak *et al.*, Phys. Rev. C **71**, 054319 (2005).
[5] M. Sandzelius *et al.*, Phys. Rev. C **80**, 054316 (2009).
[6] P. Möller, J. R. Nix, W. D. Myers, and W. J. Swiatecki, At. Data Nucl. Data Tables **59**, 185 (1995).
[7] C. W. Beausang and J. Simpson, J. Phys. G **22**, 527 (1996).
[8] C. W. Beausang *et al.*, Nucl. Instrum. Methods Phys. Res., Sect. A **313**, 37 (1992).
[9] M. Leino *et al.*, Nucl. Instrum. Methods Phys. Res., Sect. B **99**, 653 (1995).
[10] R. D. Page *et al.*, Nucl. Instrum. Methods Phys. Res., Sect. B **204**, 634 (2003).
[11] I. H. Lazarus *et al.*, IEEE Trans. Nucl. Sci. **48**, 567 (2001).
[12] K.-H. Schmidt *et al.*, Phys. Lett. B **168**, 39 (1986).
[13] R. S. Simon *et al.*, Z. Phys. A **325**, 197 (1986).
[14] E. S. Paul *et al.*, Phys. Rev. C **51**, 78 (1995).
[15] A. Keenan *et al.*, Phys. Rev. C **63**, 64309 (2001).
[16] R. D. Page *et al.*, Phys. Rev. C **53**, 660 (1996).
[17] E. Hagberg, X. J. Sun, V. T. Koslowsky, H. Schmeing, and J. C. Hardy, Phys. Rev. C **45**, 1609 (1992).
[18] S. Hofmann, W. Faust, G. Münzenberg, W. Reisdorf, and P. Armbruster, Z. Phys. A **291**, 53 (1979).
[19] E. Runte, T. Hild, W.-D. Schmidt-Ott, U. J. Schrewe, P. Tidemand-Petersson, and R. Michaelsen, Z. Phys. A **324**, 119 (1986).
[20] P. Rahkila, Nucl. Instrum. Methods Phys. Res., Sect. A **595**, 637 (2008).
[21] K. Y. Ding *et al.*, Phys. Rev. C **62**, 034316 (2000).
[22] A. Gavron, Phys. Rev. C **21**, 230 (1980).
[23] O. B. Tarasov, Nucl. Instrum. Methods Phys. Res., Sect. B **204**, 174 (2003).
[24] D. C. Radford, Nucl. Instrum. Methods Phys. Res., Sect. A **361**, 297 (1995).
[25] K. S. Krane, R. M. Steffen, and R. M. Wheeler, Nucl. Data Tables A **11**, 351 (1973).
[26] K. Theine *et al.*, Nucl. Phys. A **536**, 418 (1992).
[27] D. G. Roux *et al.*, Phys. Rev. C **63**, 024303 (2001).
[28] F. Dönau and S. Frauendorf, in *Proceedings of the Conference on High Angular Momentum Properties of Nuclei, Oak Ridge*, edited by N. R. Johnson (Harwood, New York, 1983), p. 143.
[29] F. Dönau, Nucl. Phys. A **471**, 469 (1987).
[30] R. Bengtsson and S. Frauendorf, Nucl. Phys. A **327**, 139 (1979).
[31] S. M. Harris, Phys. Rev. **138**, B509 (1965).
[32] D. G. Roux *et al.*, Phys. Rev. C **63**, 069901(E) (2001).
[33] G. D. Dracoulis *et al.*, in *Proceedings of the International Conference of Nuclear Structure at High Angular Momentum, Ottawa (1992)*, AECL Report No. 10613 (unpublished), Vol. 2, p. 94 (private communication).
[34] J. Simpson *et al.*, J. Phys. G **17**, 511 (1991).
[35] J. Thomson *et al.*, Phys. Rev. C **81**, 014307 (2010).
[36] Y. S. Chen, S. Frauendorf, and G. A. Leander, Phys. Rev. C **28**, 2437 (1983).
[37] A. J. Kreiner, M. A. J. Mariscotti, C. Baktash, E. der Mateosian, and P. Thieberger, Phys. Rev. C **23**, 748 (1981).
[38] M. Sandzelius *et al.*, Phys. Rev. C **75**, 054321 (2007).
[39] R. A. Bark *et al.*, Nucl. Phys. A **657**, 113 (1999).
[40] D. T. Joss *et al.*, Phys. Rev. C **68**, 014303 (2003).
[41] X. H. Zhou *et al.*, Eur. Phys. J. A **19**, 11 (2004).
[42] S. Frauendorf and F. R. May, Phys. Lett. B **125**, 245 (1983).
[43] E. S. Paul, C. W. Beausang, D. B. Fossan, R. Ma, W. F. Piel Jr., P. K. Weng, and N. Xu, Phys. Rev. C **36**, 153 (1987).
[44] R. Wyss, J. Nyberg, A. Johnson, R. Bengtsson, and W. Nazarewicz, Phys. Lett. B **215**, 211 (1988).